AGU PUBLICATIONS

JGR

Journal of Geophysical Research: Oceans

RESEARCH ARTICLE

10.1002/2017JC013435

Key Points:
- Rapid storm intensification and rapid decline of major tropical cyclones are analyzed in connection with the state of the sea surface
- The two-phase environment at the air-sea interface can result in the observed hysteresis of intensification and decline of tropical cyclones
- Rapid intensification, decline, and bimodal distribution of maximum intensity can be related to the aerodynamic drag well near 60 m s^{-1} wind

Correspondence to:
A. V. Soloviev,
soloviev@nova.edu

Citation:
Soloviev, A. V., Lukas, R., Donelan, M. A., Haus, B. K., & Ginis, I. (2017). Is the state of the air-sea interface a factor in rapid intensification and rapid decline of tropical cyclones? *Journal of Geophysical Research: Oceans*, *122*, 10,174–10,183. https://doi.org/10.1002/2017JC013435

Received 5 SEP 2017
Accepted 1 DEC 2017
Accepted article online 11 DEC 2017
Published online 28 DEC 2017

Is the State of the Air-Sea Interface a Factor in Rapid Intensification and Rapid Decline of Tropical Cyclones?

Alexander V. Soloviev[1,2], Roger Lukas[3], Mark A. Donelan[2], Brian K. Haus[2], and Isaac Ginis[4]

[1]Halmos College of Natural Sciences and Oceanography, Nova Southeastern University, Dania Beach, FL, USA, [2]Rosenstiel School of Marine and Atmospheric Science, University of Miami, Miami, FL, USA, [3]School of Ocean and Earth Sciences and Technology, University of Hawaii at Manoa, Honolulu, HI, USA, [4]Graduate School of Oceanography, University of Rhode Island, Narragansett, RI, USA

Abstract Tropical storm intensity prediction remains a challenge in tropical meteorology. Some tropical storms undergo dramatic rapid intensification and rapid decline. Hurricane researchers have considered particular ambient environmental conditions including the ocean thermal and salinity structure and internal vortex dynamics (e.g., eyewall replacement cycle, hot towers) as factors creating favorable conditions for rapid intensification. At this point, however, it is not exactly known to what extent the state of the sea surface controls tropical cyclone dynamics. Theoretical considerations, laboratory experiments, and numerical simulations suggest that the air-sea interface under tropical cyclones is subject to the Kelvin-Helmholtz type instability. Ejection of large quantities of spray particles due to this instability can produce a two-phase environment, which can attenuate gravity-capillary waves and alter the air-sea coupling. The unified parameterization of waveform and two-phase drag based on the physics of the air-sea interface shows the increase of the aerodynamic drag coefficient C_d with wind speed up to hurricane force ($U_{10} \approx 35$ m s^{-1}). Remarkably, there is a local C_d minimum—"an aerodynamic drag well"—at around $U_{10} \approx 60$ m s^{-1}. The negative slope of the C_d dependence on wind-speed between approximately 35 and 60 m s^{-1} favors rapid storm intensification. In contrast, the positive slope of C_d wind-speed dependence above 60 m s^{-1} is favorable for a rapid storm decline of the most powerful storms. In fact, the storms that intensify to Category 5 usually rapidly weaken afterward.

1. Introduction

Tropical storms have intrinsic predictability timescale limits (Emanuel et al., 2004; Leslie et al., 1998). Within these limits, tropical cyclone forecasts depend on the principle factors including computer power, observational constraints, and the understanding of tropical cyclone physics. During the previous decades, computer performance has increased by several orders of magnitude. Tropical cyclone observations have significantly improved as well. Storm intensity forecasting has nevertheless had almost no progress (Kaplan et al., 2010; Rogers et al., 2013). Substantial improvements in computer performance and observational capabilities indicate that key physics are poorly parameterized or missing in tropical cyclone prediction systems (Soloviev et al., 2014).

Following Emanuel (1995), Wing et al. (2007), and Lin et al. (2013), the theoretical maximum, or potential intensity (PI), of a steady state tropical cyclone is

$$V^2 = (k^* - k)\frac{(\bar{T} - T_0)}{T_0}\frac{C_k}{C_d}, \tag{1}$$

which is proportional to the enthalpy coefficient C_k and inversely proportional to the drag coefficient C_d, where V is the maximum 1 min average wind speed at 10 m height, k is the enthalpy, and k^* is the saturation enthalpy at the sea surface,

$$\bar{T} = \frac{1}{h}\int_{-h}^{0} T dz, \tag{2}$$

is defined as the precyclone depth-averaged ocean temperature, h is the 26°C isotherm depth, and T_0 is the outflow temperature at the top of the tropical cyclone determined by the atmospheric environmental

vertical temperature profile. Equation (2) reflects the importance of the heat content of the upper ocean on hurricane intensity (Shay, 2010; Shay et al., 1989).

According to equation (1), the PI index is proportional to $(C_k/C_d)^{1/2}$, thus controlling the maximum tropical cyclone intensity for given external variables (Green & Zhang, 2013). Jeong et al. (2012) found that C_k may not strongly depend on wind speed for winds $U_{10} > 10$ m s^{-1} at 10 m height. The Jeong et al. (2012) laboratory experiment was, however, limited to the maximum equivalent neutral wind speed of $U_{10}=40$ m s^{-1}. This laboratory result is in part corroborated by aircraft-based flux measurements (Drennan et al., 2007) and has been extended by Richter and Stern (2014) to $U_{10}=70$ m s^{-1} using dropsonde data. There are, however, virtually no data on C_k for higher wind speeds.

In a laboratory study, Donelan et al. (2004) found that C_d has a tendency to increase with wind speed and then level off above $U_{10} \approx 33$ m s^{-1}, corresponding to a Category 1 hurricane. The field data of Powell et al. (2003), Black et al. (2007), Jarosz et al. (2007), Bell et al. (2012), and Hsu et al. (2017) suggest that in tropical cyclones C_d levels off or even decreases above 30 m s^{-1}. Soloviev et al. (2014) concluded that the dependence of the drag coefficient on wind speed may have a local minimum around $U_{10} \approx 60$ m s^{-1} ("sweet spot" or "aerodynamic drag well").

In tropical cyclones, the air and sea are strongly coupled. Heat energy is supplied to tropical cyclones by the overheated upper ocean through the air-sea interface. Tropical cyclones also transfer momentum to and dissipate kinetic energy in the ocean through the air-sea interface.

Tropical cyclones typically undergo rapid intensification before reaching the status of a major storm. The process of rapid intensification is still a serious challenge for tropical cyclone prediction because the physics of rapid intensification are not yet completely understood (Emanuel, 1995; Kaplan et al., 2010; Lin et al., 2013). Here, we analyze the processes of rapid storm intensification and decline in connection to physical properties of the air-sea interface.

Our paper is organized as follows. Section 2 describes properties of the air-sea interface under tropical cyclones and the related numerical and laboratory experiments. In section 3, the aerodynamic drag coefficient under tropical cyclones and the theoretical background for the drag coefficient minimum at $U_{10} \approx 60$ m s^{-1} ("aerodynamic drag well") are presented. Section 4 analyzes the process of rapid intensification and decline of a number of major tropical cyclones. Possible connections between the rapid storm intensification, the peak on the histogram of the lifetime maximum intensity, and the wind speed dependence of C_d are discussed in section 5. Section 6 concludes the article.

2. The State of the Air-Sea Interface Under Tropical Cyclones

Under tropical cyclone conditions, the sea surface is covered with "white out" (Holthuijsen et al., 2012). The white out consists of foam, spray (small droplets), and spume (large droplets). The exploding air-bubbles also produce a population of small spray droplets. The white out is much more widespread than the whitecaps formed by the breaking of energy-containing surface waves. Analyzing hurricane hunter photos, Holthuijsen et al. (2012) found that the whitecap coverage in tropical cyclone conditions is less than 10% on average. They, however, did not provide any physical explanation of this phenomenon.

Physics of the air-sea interface under tropical cyclone conditions are complicated due to a wide range of time and length scales involved. The role of the two-phase environment at the air-sea interface has not yet been completely understood, which is particularly due to insufficient in situ observations.

The mechanisms that control disruption of the air-sea interface, generation of marine spray, and foam formation are somewhat analogous to the process of atomization in engineering applications, such as fuel injection in combustion and cryogenic rocket engines, food processing, and inkjet printing (Ling et al., 2015; Shinjo & Umemura, 2010; Yecko et al., 2002). Based on this analogy, the white out covering the sea surface under tropical cyclone conditions can be a result of the Kelvin-Helmholtz (KH) shear instability of the air-sea interface (Soloviev et al., 2014). This type of instability may include the well-known interfacial mode (Helmholtz, 1868; Thomson [Kelvin], 1871) and a "liquid" mode. The liquid mode develops in the two-phase viscous mixing layers at the gas-liquid interface. The liquid mode may have some resemblance to the Holmboe (1962) instability. The Holmboe instability appears in a number of atmospheric, oceanic, and

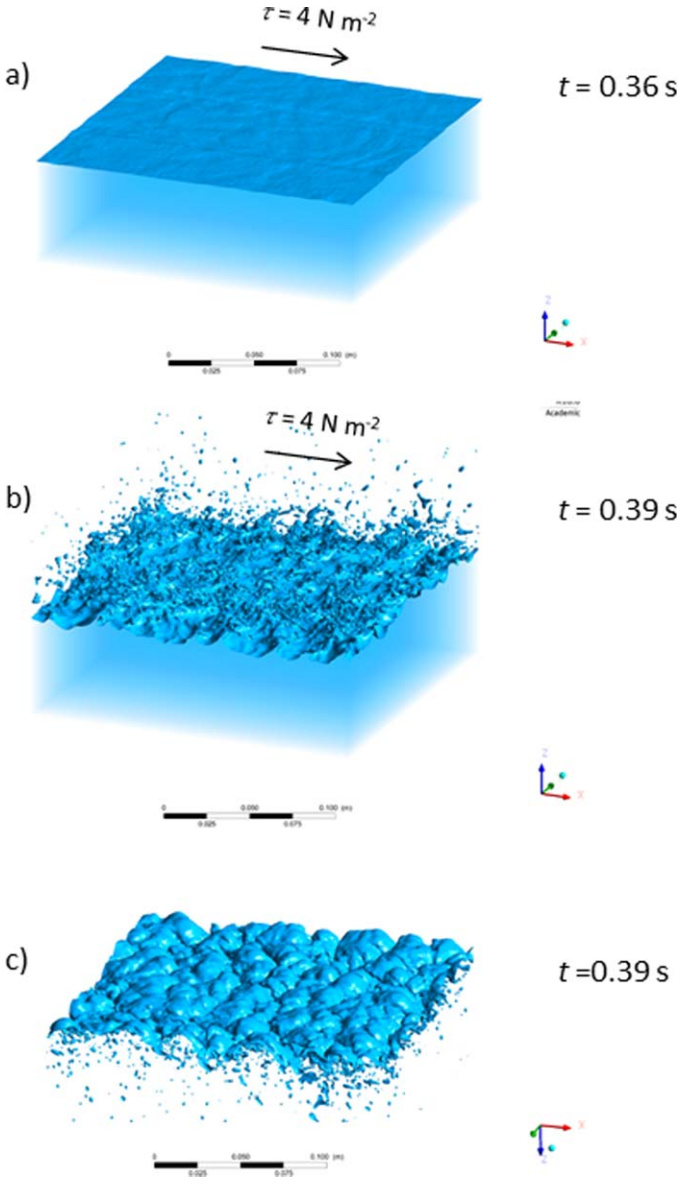

Figure 1. The air-sea interface under hurricane force wind simulated with a VOF LES model. (a) The wind stress reached the water surface at $t = 0.36$ s and (b) triggered the KH instability, which was fully developed at $t = 0.39$ s. (c) View of the air-water interface from below.

astrophysical problems (Alexakis, 2007; Constantinoua & Ioannoub, 2011; Smyth, 2006; Smyth & Peltier, 1989). The Holmboe instability can develop in highly stratified shear layers when the density stratification is concentrated in a small region of the shear layer. The Holmboe instability mode has not been studied in detail in the case of the air-water interface. The initial instability may occur in the form of the interfacial (KH) mode and then transit into a Holmboe mode (Smyth & Winters, 2003).

Terminology in this area of science has not yet been finalized. To be consistent with the literature on atomization (see, e.g., Jerome et al., 2013; Ling et al., 2015; and others), we will call both the interfacial and liquid instability modes the KH instability.

Under light winds, the KH instability of the air-water interface may contribute to the generation of surface waves in the gravity-capillary range. Under slightly stronger wind speed conditions, these waves become steep, nonlinear, and break internally (i.e., without piercing the air-water interface). This phenomenon is called "microscale wave breaking" (Banner & Phillips, 1974). For winds greater than $\sim$6 m s^{-1}, gravity waves break and wind flow separation from the surface becomes an issue. Under strong winds, around $U_{10} \approx 30$ m s^{-1}, the microscale wave breaking overcomes gravity and surface tension forces and disrupts the air-sea interface (Hoepffner et al., 2011; Soloviev & Lukas, 2010). As a result, intense formation of foam, spume, and marine spray occurs, which may contribute to most of the white out cover of the sea surface under tropical cyclone conditions.

Figure 1 shows the results of a numerical experiment performed with the multiphase volume of fluid large eddy simulation (VOF LES) computational fluid dynamics model described in Soloviev et al. (2012). A very fine mesh with the spatial resolution at the air-water interface $\Delta x \times \Delta y \times \Delta z = 0.75 \times 0.75 \times 0.75$ mm^3 was used in this work (versus $5.0 \times 5.0 \times 1.0$ mm^3 in Soloviev et al., 2012). The surface tension coefficient at the air-water interface was set at 0.072 N m^{-1}; periodic boundary conditions were set along the x axis; and slippery boundary conditions at the bottom and side walls.

The model (Figure 1) was initialized with a flat air-sea interface. The model was forced with a 4 N m^{-1} wind stress corresponding to $U_{10} \approx 40$ m s^{-1} (a and b) and applied as a boundary condition at the top of the numerical domain. Figure 1c views the sea surface from below. There is a noticeable asymmetry between the air and water sides of the interface—most of the action is on the airside. Such asymmetry is typical for the KH instability at an interface between liquids with a significant density difference (Hoepffner et al., 2011).

In the view from below (Figure 1c), there are "loops" at the sea surface. We interpret these structures as the possible signature of the Holmboe instability mode (Smyth & Winters, 2003). The Holmboe mode for very strong stratification is characterized by periodic ejections of the loops far away from the shear layers as a result of the sloping convection (Emanuel, 1994; Smyth, 2006). This is a plausible mechanism for the formation of finger-shaped (Koga, 1981) and bag-shaped structures (Troitskaya et al., 2017), which are responsible for the production of sea spray, foam, and spume under tropical cyclone conditions.

The laboratory experiments conducted at the University of Miami Rosenstiel School of Marine and Atmospheric Science (UM RSMAS) ASIST facility have revealed features of various shapes above the water surface, generating sea spray, and spume (Figure 2) that are qualitatively consistent with the results of numerical simulations. Note that numerical simulation of foam requires much finer mesh resolution.

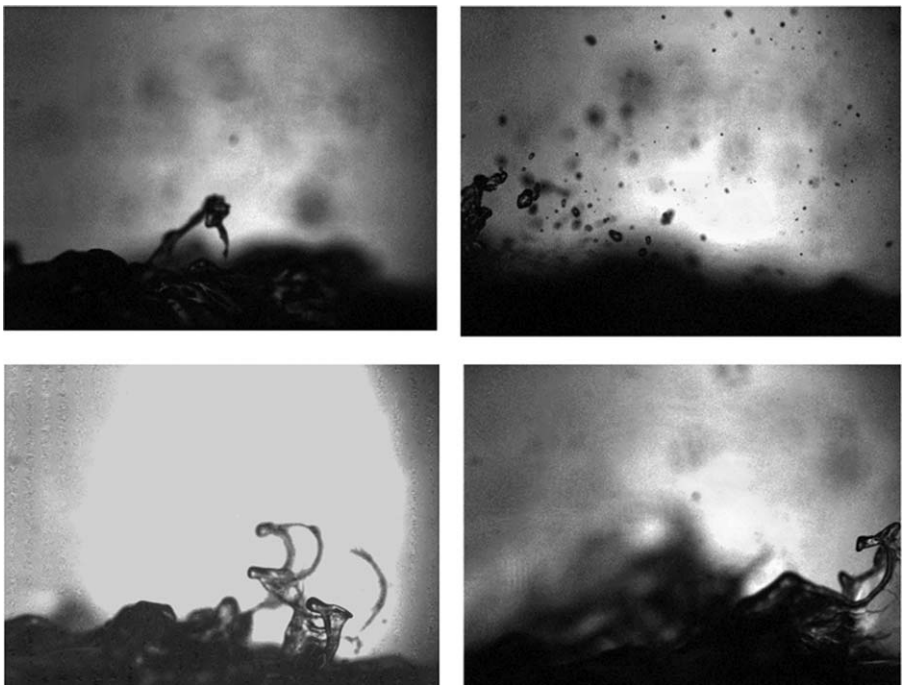

Figure 2. Disruptions of the air-water interface under hurricane-force wind revealed with shadow-imaging techniques. The equivalent wind speed is $U_{10} = 40$ m s^{-1} (equivalent to a Category 2 tropical cyclone). This laboratory experiment was conducted at the UM RSMAS ASIST facility (Soloviev et al., 2014). The large difference in density between the air and water leads to strong asymmetry of the KH instability process (Hoepffner et al., 2011). Note that the shadow imaging technique used for visualization in this experiment could not resolve air bubbles in the water. (top) Finger-type ejection from the surface and (bottom) bag development from looped structures. According to the laboratory experiment conducted by Troitskaya et al. (2017), spray generation by the bag structures dominated over that of the fingers (the laboratory conditions corresponded to a Category 1 storm).

Miles' (1959) theoretical analysis demonstrated that the KH instability could develop at a flat air-water interface but not in the presence of wind waves. Nevertheless, Koga (1981) reported observations of the KH instability at the air-water interface in a laboratory study performed under a hurricane force wind in the presence of surface waves. In Koga's experiment, the KH instability was observed predominantly near wave crests. The numerical simulation in the presence of a surface wave (Figure 3) reveals the KH instability as well, predominately near wave crests, corroborating Koga's laboratory result.

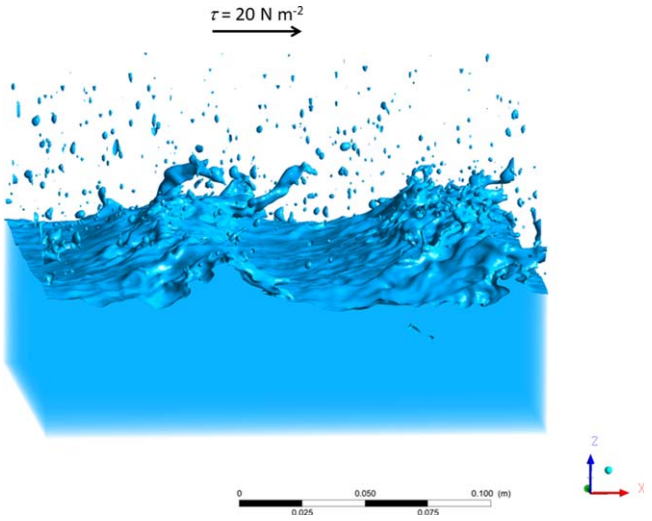

Figure 3. The air-water interface under tropical cyclone wind stress in the presence of a surface wave (simulated with the same multiphase model as in Figure 1).

In order to explain these laboratory and numerical results (which differ from Miles' 1959 prediction) for the case shown in Figures 1a and 1b, we traced the development of the KH instability from the initially flat air-sea interface (Figure 1a) to a stage of developed KH instability (Figure 1b). The wind stress applied to the top of the numerical domain as a boundary condition at t = 0 s, penetrated to the air-water interface at t = 0.36 s (Figure 1a). Remarkably, it took only O(10^{-2} s) to develop the KH instability.

Miles (1959) considered only the time-averaged wind velocity profile. As we see from the numerical experiment shown in Figures 1a and 1b, the KH instability can develop on a time scale much less than the period of energy-containing wind waves. This result is consistent with Kelly's (1965) theoretical estimate for the time scale of the KH instability development at the air-water interface.

When waves are present, the instantaneous wind velocity profile significantly fluctuates near the sea surface. As a result, the interfacial

shear fluctuates and can reach much larger values than the time-averaged shear, especially near the wave crests. Consequently, the KH instability of the air-sea interface has sufficient time to develop in response to a local increase of the wind shear on the wave profile, locally disrupting the interface, producing foam, spume, and a spectrum of small droplets. This is an example of the hydrodynamic system that is stable on average but unstable for fluctuations (Farrell & Ioannou, 2008).

3. Drag Coefficient in Two-Phase Environment

Several laboratory and field experiments have reported the leveling off or decreasing of C_d under very high wind-speed conditions (Bell et al., 2012; Black et al., 2007; Donelan et al., 2004; Hsu et al., 2017; Jarosz et al., 2007; Powell et al., 2003). This phenomenon cannot be explained by the suppression of near-surface turbulence by buoyancy forces due to spray loading in the hurricane boundary layer. With the currently known sea spray generation function, the spray buoyancy effect on C_d (referred to 10 m height) appears to be relatively small (Ingel, 2011; Soloviev & Lukas, 2006), though it may be more pronounced at greater heights above the sea surface.

Some useful conclusions can be derived based on analogies with other areas of science. Soloviev & Lukas (2010) proposed to treat the two-phase layer at the air-water interface as the transitional boundary layer in a self-regulating regime, which maintains the Richardson number near its critical value. The elimination of short surface waves by the KH instability of the air-sea interface reduces the wave-induced aerodynamic drag, while the two-phase environment produces additional drag. The latter, however, becomes significant only under conditions of major tropical cyclones.

Figure 4 shows the unified parameterization of air-sea drag coefficient including the waveform induced drag and the two-phase drag (Soloviev et al., 2014). This parameterization is consistent with the available observational data on the drag coefficient in tropical cyclones (Bell et al., 2012; Black et al., 2007; Jarosz et al., 2007; Powell et al., 2003). New observational data (Hsu et al., 2017), obtained from the ocean current response which clearly shows a decrease in the drag coefficient, have been added for comparison. Zhao et al. (2015) measured the typhoon air-sea drag coefficient from a coastal tower located in the South China Sea for wind speeds up to 50 m s^{-1}. Their data, after extrapolation to open ocean conditions, are consistent with the unified parameterization shown in Figure 4.

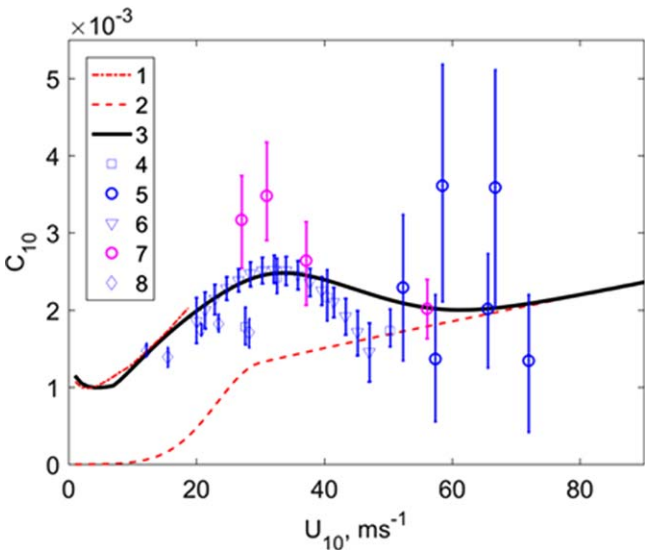

Figure 4. The unified air-sea drag coefficient parameterization. Available observations (only those containing confidence intervals) are also included. Lines and symbols indicate: 1, Fairall's et al. (2003) COARE 3.0 algorithm; 2, Soloviev and Lukas's (2010) two-phase layer parameterization; 3, unified parameterization (Soloviev et al., 2014); 4, dropwindsondes (Powell et al., 2003); 5, angular momentum conservation (Bell et al., 2012); 6, upper ocean current response (Jarosz et al., 2007); 7, upper ocean current response (Hsu et al., 2017); and 8, dropwindsondes (Black et al., 2007).

According to the unified parameterization (Figure 4), the drag coefficient increases with wind speed up to ~35 m s^{-1}. The drag coefficient levels off around 35 m s^{-1}, then drops with the slope being negative until about 60 m s^{-1}, where it increases again.

The leveling off around $U_{10} \approx 35$ m s^{-1} and subsequent decrease of the drag coefficient with increasing wind speed is due to the progressively stronger disruption of gravity-capillary waves at the air-sea interface by the KH instability (Soloviev & Lukas, 2010). The two-phase layer at the air-water interface cannot support the surface waves whose wavelengths are shorter than or comparable to its thickness. Suppression of short surface waves results in a reduced aerodynamic resistance of the sea surface to the wind.

Above 60 m s^{-1}, the aerodynamic drag again increases due to the growing presence of the two-phase layer taking momentum from the air (see the two-phase drag parameterization in Figure 4). As a result, a local drag coefficient minimum—the aerodynamic drag well—remarkably develops around $U_{10} \approx 60$ m s^{-1} (Figure 4). The corresponding minimum for the wind stress is somewhat less pronounced than that for the drag coefficient. Nevertheless, according to equation (1), the PI is proportional to the drag coefficient, while the wind stress does not explicitly enter this equation.

In the following section, we investigate likely consequences of this feature for tropical cyclone dynamics.

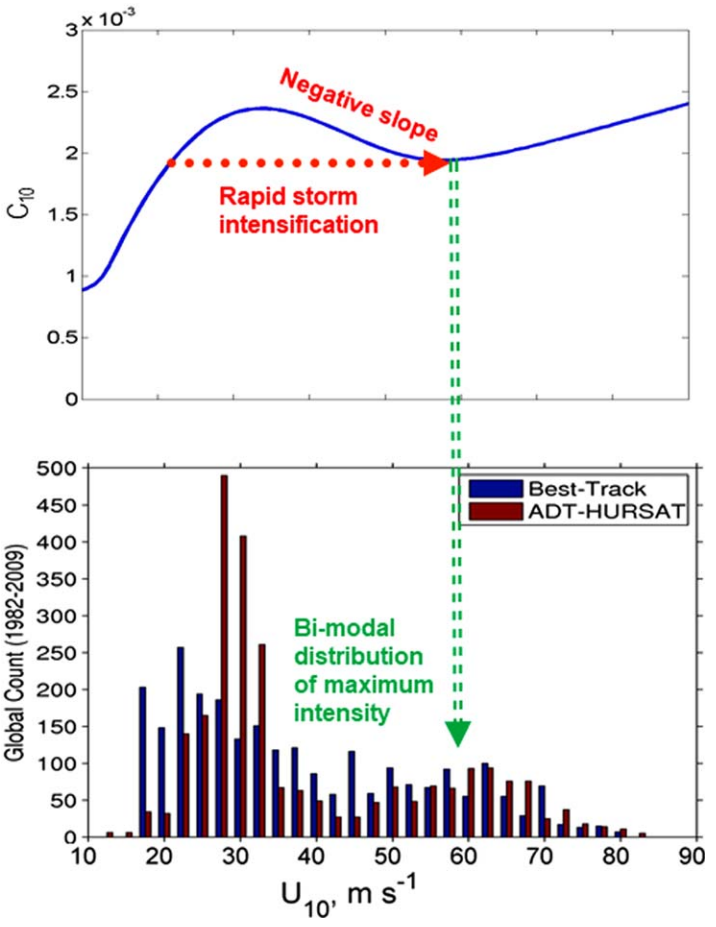

Figure 5. (top) The shape of C_d containing the aerodynamic drag well around 60 m s^{-1} wind speed can explain rapid intensification and (bottom) the bimodal distribution of lifetime maximum intensity for tropical cyclones reported by Kossin et al. (2013).

4. Rapid Storm Intensification and Weakening

Rapid storm intensification is defined as a tropical cyclone intensity increase of at least 15.4 m s^{-1} in 24 h (Wang et al., 2015). Respectively, we define rapid storm decline as a tropical cyclone weakening by at least 15.4 m s^{-1} in 24 h.

Under the assumption of a nearly constant enthalpy coefficient, the decrease of the drag coefficient from 35 to 60 m s^{-1} is favorable for rapid storm intensification (Figure 5). However, for tropical storm strength winds, a significant wind-speed fluctuation is necessary to surmount the peak value of C_d around 35 m s^{-1}. Only a relatively small number of storms is able to make it over this barrier and reach the wind-speed range with favorable sea surface conditions (the negative slope of the drag wind-speed dependence between 35 and 60 m s^{-1}).

The positive slope of the $C_d(U_{10})$ dependence on wind speed above 60 m s^{-1} is not favorable for further storm intensification, which may explain why only a relatively small number of tropical cyclones reach Category 5. The positive slope of the C_d dependence above 60 m s^{-1} is not favorable for further storm intensification, because the increasing friction at the sea surface, possibly, destabilizes the vortex and initiates the eyewall replacement cycle, leading to the rapid decline of the tropical cyclones that previously reached Category 5 status.

The presence of the aerodynamic drag well around 60 m s^{-1} wind speed leads to an increased probability for a tropical cyclone to stay near this intensity. This condition is consistent with the multiyear statistics of tropical cyclones showing the secondary peak on the histogram of lifetime maximum intensity (Figure 5). Soloviev et al. (2014) and Lee et al. (2016) have also linked this peak to the process of rapid intensification.

Figure 6 shows a comparison of the theoretical unified drag coefficient with the rate of intensification of Category 4 hurricanes and tropical cyclones as a function of wind speed. Rapid intensification apparently happened for those storms that were able to overcome the positive slope of C_d between approximately 30 and 35 m s^{-1} wind speed. The data in Figure 6 are taken from Category 4 storms when they were within the tropics and away from land.

In Figure 7, a similar comparison is shown for Category 5 storms. These data are taken from the Category 5 storms when they were within the tropics and away from land. After the rapid intensification stage, these storms continued intensification to Category 5 storms. Remarkably, practically all storms that had reached Category 5 status then rapidly declined ("bounced") to Category 3 or so storms. This behavior of Category 5 tropical cyclones can qualitatively be explained by the presence of the aerodynamic drag well at 60 m s^{-1} wind speed. This is also consistent with the multiyear statistics of tropical cyclones containing the peak of the lifetime maximum intensity around the 60 m s^{-1} wind speed (Figure 5).

5. Discussion

The maximum lifetime intensity has been linked to the PI index defined by equation (1) (Emanuel, 1995; Lin et al., 2013; Shay, 2010). Emanuel (2000) concluded that ". . .a given storm is equally likely to attain any intensity up to its PI." The intensity of a storm moving over regions with the different PI depends on the time needed for the storm to adjust to the new environmental conditions (Wing et al., 2007). The shape of the air-sea drag coefficient including the aerodynamic drag well (Figure 8) can result in a nonlinear, hysteresis-type response of the moving storm to changing environmental conditions.

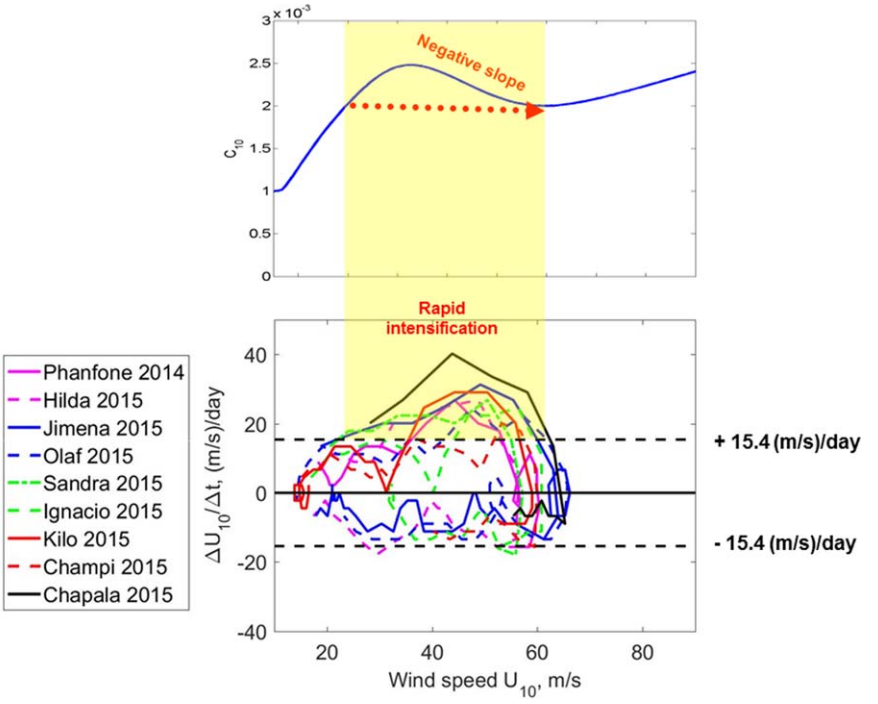

Figure 6. (top plot) The air-sea drag coefficient as a function of wind speed for open ocean hurricanes and tropical cyclones that reached Category 4; (bottom plot) observed rate of wind speed change $\Delta U_{10}/\Delta t$ in m s^{-1} d^{-1} as a function of wind speed U_{10} in m s^{-1}. Rapid intensification threshold is shown by a dashed line $\Delta U_{10}/\Delta t = 15.4$ m s^{-1} d^{-1}. Rapid decline threshold is shown by a dashed line $\Delta U_{10}/\Delta t = -15.4$ m s^{-1} d^{-1}.

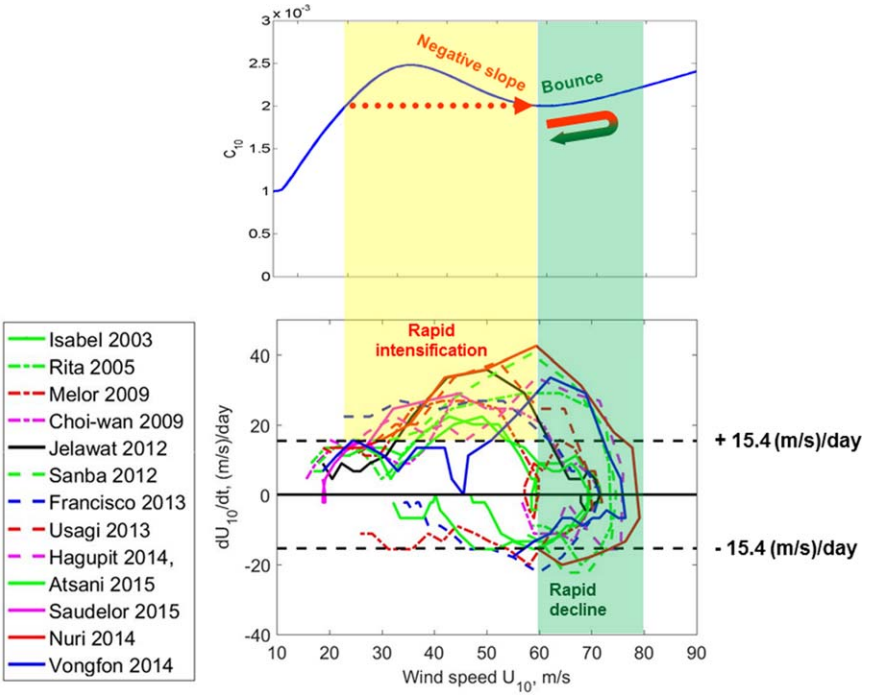

Figure 7. (top plot) The air-sea drag coefficient as a function of wind speed for open ocean hurricanes and tropical cyclones that reached Category 5 intensity; (bottom plot) observed rate of wind speed change $\Delta U_{10}/\Delta t$ in (m s^{-1}) d^{-1} as a function of wind speed U_{10} in m s^{-1}. Rapid intensification threshold is shown by a dashed line $\Delta U_{10}/\Delta t = 15.4$ m s^{-1} d^{-1}. Rapid decline threshold is shown by a dashed line $\Delta U_{10}/\Delta t = -15.4$ m s^{-1} d^{-1}.

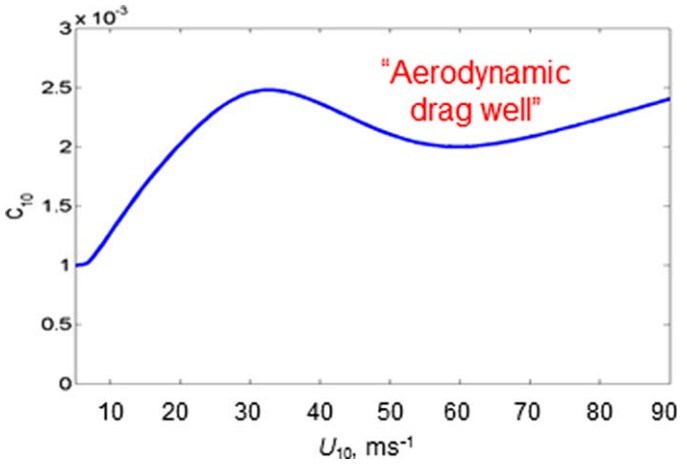

Figure 8. The aerodynamic drag well around 60 m s^{-1} in the theoretical unified drag parameterization (Soloviev et al., 2014) potentially explaining rapid intensification and rapid decline of tropical storms. The negative slope of C_d above 35 m s^{-1} is due to progressive loss of form drag as short surface waves cease to exist due to the KH instability of the air-sea interface and increasing thickness of the two-phase near-surface layer. As this layer thickens, the two-phase drag increases rapidly, limiting the strength of tropical cyclones.

Emanuel (2000) reported hysteresis in the average hurricane intensity. The intensity declined at roughly two-thirds of its prior intensification rate. Asymmetries including rapid intensification and rapid decline of tropical cyclones demonstrated in Figures 6 and 7 are examples of such hysteresis as well.

The negative slope of the aerodynamic drag coefficient between 35 and 60 m s^{-1} wind speed can explain the rapid intensification of some tropical cyclones. Further intensification of the storm can take place if the PI index allows it. However, the storms that reach a Category 5 intensity at some point can quickly "bounce" to the Category 3 or so intensity due to positive slope of the aerodynamic drag coefficient with wind above 60 m s^{-1}. We call this the rapid decline of the tropical cyclone.

A typical feature of major hurricanes and tropical cyclones is the eyewall replacement cycle. Storm intensity usually decreases during the eyewall replacement cycle (DeMaria et al., 2005; Houze et al., 2007; Knaff et al., 2003; Kossin & Sitkowski, 2009; Terwey & Montgomery, 2006; Willoughby, 1990). The intensity weakens due to the instability and gradual erosion of the inner eyewall. The process of the eyewall replacement has been observed in detail (Cione et al., 2013, Kossin, 2015; Sitkowski et al., 2012) but the underlying physics has not yet been completely understood. A hypothesis resulting from our research is that the state of the surface may play a role in the eyewall replacement cycle. The eyewall instability can in principle develop due to the increased aerodynamic drag on the sea surface above 60 m s^{-1} wind speed, with the new eyewall developing in the region of lower winds within the aerodynamic drag well.

6. Conclusions

Observations show that most major tropical cyclones undergo rapid intensification. Notably, after achieving maximum intensity, most Category 5 storms experience rapid decline to Category 3. These processes are not yet well understood. In this work, we have analyzed the state of the sea surface as a factor in rapid storm intensification and rapid storm decline. Theoretical analysis, laboratory experiments, and numerical simulations have demonstrated that the air-water interface under tropical cyclones is expected to develop the KH shear instability, producing the two-phase layer suppressing short surface waves and thus altering the aerodynamic properties of the sea surface. However, under major tropical cyclones, this intermediate two-phase layer can notably add to the aerodynamic drag due to the additional momentum required for acceleration of the sea spray and spume drops.

The parameterization unifying the waveform drag and two-phase environment drag (Figure 4) shows the drag coefficient (C_d) increasing with wind speed, up to ~35 m s^{-1}. The parameterization reveals a local minimum of the drag coefficient (the aerodynamic drag well) around 60 m s^{-1}. Such shape of the drag coefficient dependence on wind speed can explain the rapid intensification and rapid decline of hurricanes and tropical cyclones. In fact, under the assumption of a constant enthalpy exchange coefficient, the negative slope of the C_d dependence on wind speed within the range of approximately 35–60 m s^{-1} is conducive to rapid storm intensification. Respectively, the positive slope of the C_d wind-speed dependence above approximately 60 m s^{-1} supports rapid storm decline. Increasing aerodynamic drag of the sea surface above 60 m s^{-1} wind speed can also be responsible for the eyewall instability and replacement. Finally, the secondary peak in the multiyear statistics of lifetime maximum intensity of tropical cyclones around 60 m s^{-1} wind speed is consistent with the presence of the aerodynamic well.

There has been significant progress in studying the air-sea interaction in major tropical cyclones, which includes moored buoy data (e.g., Cione et al., 2013), Argo floats (e.g., Riser et al., 2016), and the ONR-sponsored Impact of Typhoon on Pacific (ITOP) experiment (D'Asaro et al., 2014). There are nevertheless still very scarce data on the state of the air-sea interface in major tropical cyclones, especially in Category 5 storms. (This is the reason that we have based this work on the laboratory and numerical experiments.)

Potentially, high-resolution SAR imagery in L-band may give additional and valuable information on the sea surface state in major tropical cyclones.

Acknowledgments
Mike McGauley and Cayla Dean (NSU) helped with numerical simulations. Kathryn Howe (NSU) helped with data collection; and, Luba Solonenko (NSU) with manuscript preparation. This research was made possible by the Gulf of Mexico Research Initiative (Grant SA-1515 CARTHE) and NOAA award NA15OAR4310173. Metadata on the laboratory experiments are available on https://data.gulfresearchinitiative.org/data/R1.x134.073:0009. Data on hurricanes and tropical cyclones were taken from https://www.wunderground.com/hurricane.

References

Alexakis, A. (2007). Marginally unstable Holmboe modes. *Physics of Fluids*, *19*, 054105.
Banner, M. L., & Phillips, O. M. (1974). On the incipient breaking of small scale waves. *Journal of Fluid Mechanics*, *65*, 647–656.
Bell, M. M., Montgomery, M. T., & Emanuel, K. A. (2012). Air–sea enthalpy and momentum exchange at major hurricane wind speeds observed during CBLAST. *Journal of Atmospheric Sciences*, *69*, 3197–3222.
Black, P. G., D'asaro, E. A., Drennan, W. M., French, J. R., Niiler, P. P., Sanford, T. B., . . . Zhang, J. A. (2007). Air-Sea exchange in hurricanes: synthesis of observations from the coupled boundary layer air-sea transfer experiment. *Bulletin of the American Meteorological Society*, *88*(3), 357–374.
Cione, J. J., Kalina, E. A., Zhang, J. A., & Uhlhorn, E. W. (2013). Observations of air-sea interaction and intensity change in hurricanes. *Monthly Weather Review*, *141*, 2368–2382.
Constantinoua, N. C., & Ioannoub, P. A. (2011). Optimal excitation of two dimensional Holmboe instabilities. *Physics of Fluids*, *23*, 074102.
D'Asaro, E. A., Black, P. G., Centurioni, L. R., Chang, Y.-T., Chen, S. S., Foster, R. C., . . . Wu, C.-C. (2014). Impact of typhoons on the ocean in the Pacific. *Bulletin of the American Meteorological Society*, *95*, 1405–1418.
DeMaria, M., Kaplan, J., Mainelli, M., Shay, L. K., Knaff, J. A., & Kaplan, J. (2005). Further improvements to the Statistical Hurricane Intensity Prediction Scheme (SHIPS). *Weather and Forecasting*, *20*, 531–543.
Donelan, M. A., Haus, B. K., Reul, N., Plant, W. J., Stiassne, M., Graber, H. C., . . . Saltzman, E. S. (2004). On the limiting aerodynamic roughness of the ocean in very strong winds. *Geophysical Research Letters*, *31*, L18306. https://doi.org/10.1029/2004GL019460
Drennan, W. M., Zhang, J., French, J. R., McCormick, C., & Black, P. G. (2007). Turbulent fluxes in the hurricane boundary layer. Part II: Latent heat flux. *Journal of the Atmospheric Sciences*, *64*, 1103–1115.
Emanuel, K. (1994). *Atmospheric convection*. New York, NY: Oxford University Press.
Emanuel, K. (1995). Sensitivity of tropical cyclones to surface exchange coefficients and a revised steady-state model incorporating eye dynamics. *Journal of Atmospheric Sciences*, *52*, 3969–3976.
Emanuel, K. (2000). A statistical analysis of tropical cyclone intensity. *Monthly Weather Review*, *128*, 1139–1152.
Emanuel, K. A., Des Autels, C., Holloway, C., & Korty, R. (2004). Environmental control of tropical cyclone intensity. *Journal of Atmospheric Sciences*, *61*, 843–858.
Fairall, C. W., Bradley, E. F., Hare, J. E., Grachev, A. A., & Edson, J. B. (2003). Bulk parameterization of air–sea fluxes: Updates and verification for the COARE algorithm. *Journal of Climate*, *16*, 571–591.
Farrell, B. F., & Ioannou, P. J. (2008). The stochastic parametric mechanism for growth of wind-driven surface water waves. *Journal of Physical Oceanography*, *38*, 862–879.
Green, B. W., & Zhang, E. (2013). Impacts of air–sea flux parameterizations on the intensity and structure of tropical cyclones. *Monthly Weather Review*, *141*, 2308–2324.
Helmholtz, H. (1868). Über discontinuierliche Flüssigkeits-Bewegungen [On the discontinuous movements of fluids]. *Monatsberichte der Königlichen Preussische Akademie der Wissenschaften zu Berlin*, *23*, 215–228.
Hoepffner, J., Blumenthal, R., & Zaleski, S. (2011). Self-similar wave produced by local perturbation of the Kelvin-Helmholtz shear-layer instability. *Physical Review Letters*, *106*, 104502-1–104502-4.
Holmboe, J. (1962). On the behavior of symmetric waves in stratified shear layers. *Geophysical Publications*, *24*, 67–113.
Holthuijsen, L. H., Powell, M. D., & Pietrzak, D. (2012). Wind and waves in extreme hurricanes. *Journal of Geophysical Research*, *117*, C09003. https://doi.org/10.1029/2012JC007983
Houze, R. A. Jr., Shuyi, S. C., Bradley, F., Smull1, B. F., Lee, W.-C., & Bell, M. M. (2007). Hurricane intensity and eyewall replacement. *Science*, *315*(5816), 1235–1239.
Hsu, J.-Y., Lien, R.-C., D'asaro, E. A., & Sanford, T. B. (2017). Estimates of surface wind stress and drag coefficients in Typhoon Megi. *Physical Oceanography*, *47*, 545–565.
Ingel, L. K. (2011). The effect of sea spray on the dynamics of marine atmospheric surface layer in strong winds. *Izvestiya, Atmospheric and Oceanic Physics*, *47*, 119–127.
Jarosz, E., Mitchell, D. A., Wang, D. W., & Teague, W. J. (2007). Bottom-up determination of air-sea momentum exchange under a major tropical cyclone. *Science*, *315*, 1707–1709.
Jeong, D., Haus, B. K., & Donelan, M. A. (2012). Enthalpy transfer across the air–water interface in high winds including spray. *Journal of Atmospheric Sciences*, *69*, 2733–2748.
Jerome, J. J. S., Marty, S., Matas, J.-P., Zaleski, A., & Hoepffner, J. (2013). Vortices catapult droplets in atomization. *Physics of Fluids*, *25*, 112109.
Kaplan, J., DeMaria, M., & Knaff, J. A. (2010). A revised tropical cyclone rapid intensification index for the Atlantic and Eastern North Pacific Basins. *Weather and Forecasting*, *25*, 220–241.
Kelly, R. E. (1965). The stability of an unsteady Kelvin-Helmholtz flow. *Journal of Fluid Mechanics*, *22*, 547–560.
Knaff, J. A., Kossin, J. P., & DeMaria, M. (2003). Annular hurricanes. *Weather and Forecasting*, *18*, 204–223.
Koga, M. (1981). Direct production of droplets from breaking wind-waves-Its observation by a multi-colored overlapping exposure technique. *Tellus*, *33*, 552–563.
Kossin, J. P., Olander, T. L., & Knapp, K. R. (2013). Trend Analysis with a New Global Record of Tropical Cyclone Intensity. *Journal of Climate*, *26*, 9960–9976. https://doi.org/10.1175/JCLI-D-13-00262.1
Kossin, J. P. (2015). Hurricane wind–pressure relationship and eyewall replacement cycles. *Weather and Forecasting*, *30*, 177–181.
Kossin, J. P., & Sitkowski, M. (2009). An objective model for identifying secondary eyewall formation in hurricanes. *Monthly Weather Review*, *137*(3), 876–892.
Lee, C.-Y., Tippett, M. K., Sobel, A. H., & Camargo, S. J. (2016). Rapid intensification and the bimodal distribution of tropical cyclone intensity. *Nature Communications*, *7*, 10625.
Leslie, L. M., Abbey, R. F., Jr., & Holland, G. J. (1998). Tropical cyclone track predictability. *Meteorology and Atmospheric Physics*, *65*, 223–231.
Lin, I.-I., Black, P., Price, J. F., Yang, C.-Y., Chen, S. S., Lien, C.-C., . . . D'Asaro, E. A. (2013). An ocean coupling potential intensity index for tropical cyclones. *Geophysical Research Letters*, *40*, 1878–1882. https://doi.org/10.1002/grl.50091

Ling, Y., Zaleski, S., & Scardovelli, R. (2015). Multiscale simulation of atomization with small droplets represented by a Lagrangian point-particle model. *International Journal of Multiphase Flow*, *76*, 122–143.
Miles, J. W. (1959). On the generation of surface waves by shear flows. Part 3. Kelvin-Helmholtz instability. *Journal of Fluid Mechanics*, *6*, 583–598.
Powell, M. D., Vickery, P. J., & Reinhold, T. A. (2003). Reduced drag coefficient for high wind speeds in tropical cyclones. *Nature*, *422*, 279–283. https://doi.org/10.1038/nature01481
Richter, D. H., & Stern, D. P. (2014). Evidence of spray-mediated air-sea enthalpy flux within tropical cyclones. *Geophysical Research Letters*, *41*, 2997–3003. https://doi.org/10.1002/2014GL059746
Riser, S. C., Freeland, H. J., Roemmich, D., Wijffels, S., Troisi, A., Belbéoch, M., . . . Jayne, S. R. (2016). Fifteen years of ocean observations with the global Argo array. *Nature Climate Change*, *6*, 145–153.
Rogers, R., Aberson, S., Aksoy, A., Annane, B., Black, M., Cione, J., . . . Zhang, X. (2013). NOAA's hurricane intensity forecasting experiment: A progress report. *Bulletin of the American Meteorological Society*, *94*, 859–882.
Shay, L. K. (2010). Chapter 3: Air-sea interactions in tropical cyclones. In J. C. L. Chan, J. Kepert, & C. P. Chang (Eds.), *Global perspectives of tropical cyclones, Earth System Science Publication Series*, (2nd ed., pp. 93–131) London, UK: World Scientific Publishing Company,.
Shay, L. K., Elsberry, R. L., & Black, P. G. (1989). Vertical structure of the ocean current response to a hurricane. *Journal of Physical Oceanography*, *19*, 1249– 1269.
Shinjo, J., A., & Umemura, A. (2010). Simulation of liquid jet primary breakup: Dynamics of ligament and droplet formation. *International Journal of Multiphase Flow*, *36*, 513–532.
Sitkowski, M., Kossin, J. P., Rozoff, C. M., & Knaff, J. A. (2012). Hurricane eyewall replacement cycle thermodynamics and the relict inner eyewall circulation. *Monthly Weather Review*, *140*, 4035–4045.
Smyth, W. D. (2006). Secondary circulations in Holmboe waves. *Physics of Fluids*, *18*(6), 064104.
Smyth, W. D., & Peltier, W. R. (1989). The transition between Kelvin–Helmholtz and Holmboe instability: An investigation of the overreflection hypothesis. *Journal of the Atmospheric Sciences*, *46*(24), 3698–3720.
Smyth, W. D., & Winters, K. B. (2003). Turbulence and mixing in Holmboe waves. *Journal of Physical Oceanography*, *33*, 694–711.
Soloviev, A., Fujimura, A., & Matt, S. (2012). Air-sea interface in hurricane conditions. *Journal of Geophysical Research*, *117*, C00J34. https://doi.org/10.1029/2011JC007760
Soloviev, A., & Lukas, R. (2006). *The near-surface layer of the ocean: Structure, dynamics and applications*. Berlin, Germany: Springer.
Soloviev, A., & Lukas, R. (2010). Effects of bubbles and spray on air-sea exchange in hurricane conditions. *Boundary-Layer Meteorology*, *136*, 365–376.
Soloviev, A., Lukas, R., Donelan, M., Haus, B., & Ginis, I. (2014). The air-sea interface and surface stress under tropical cyclones. *Nature Scientific Reports*, *4*, 5306.
Terwey, W. D., & Montgomery, M. T. (2006). *Modeled secondary eyewall and spiral band dynamics*. Paper presented at 27th Conference on Hurricanes and Tropical Meteorology. American Meteorological Society, Monterey, CA.
Thomson, W. (1871). Hydrokinetic solutions and observations. *The Philosophical Magazine Series* 4, 42, 362–377.
Troitskaya, Y., Kandaurov, A., Ermakova, O., Kozlov, D., Sergeev, D., & Zilitinkevich, S. (2017). Bag-breakup fragmentation as the dominant mechanism of sea-spray production in high winds. *Scientific Reports*, *7*, 1614.
Wang, X., Wang, C., Zhang, L., & Wang, X. (2015). Multidecadal variability of tropical cyclone rapid intensification in the Western North Pacific. *Journal of Climate*, *28*, 3806–3820.
Willoughby, H. E. (1990). Temporal changes of the primary circulation in tropical cyclones. *Journal of Atmospheric Sciences*, *47*, 242–264.
Wing, A. A., Sobel, A. H., & Camargo, S. J. (2007). Relationship between the potential and actual intensities of tropical cyclones on interannual time scales. *Geophysical Research Letters*, *34*, L08810. https://doi.org/10.1029/2006GL028581
Yecko, P., Zaleski, S., & Fullana, J.-M. (2002). Viscous modes in two-phase mixing layers. *Physics of Fluids*, *14*, 4115–4122.
Zhao, Z.-K., Liu, C.-X., Li, Q., Dai, G.-F., Song, Q.-T., & Lv, W.-H. (2015). Typhoon air-sea drag coefficient in coastal regions. *Journal of Geophysical Research Oceans*, *120*, 716–727. https://doi.org/10.1002/2014JC010283